J. Fluid Mech. (1999), *vol.* 393, *pp.* 59–87. Printed in the United Kingdom

The onset of chaos in a class of Navier–Stokes solutions

By PHILIP HALL[1]
AND DEMETRIOS T. PAPAGEORGIOU[2]

[1]Department of Mathematics, Imperial College of Science, Technology and Medicine, London SW7 2BZ, UK

[2]Department of Mathematical Sciences and Center for Applied Mathematics and Statistics, New Jersey Institute of Technology, University Heights, Newark, NJ 07102, USA

(Received 30 June 1997 and in revised form 1 March 1999)

The flow between parallel walls driven by the time-periodic oscillation of one of the walls is investigated. The flow is characterized by a non-dimensional amplitude Δ and a Reynolds number R. At small values of the Reynolds number the flow is synchronous with the wall motion and is stable. If the amplitude of oscillation is held fixed and the Reynolds number is increased there is a symmetry-breaking bifurcation at a finite value of R. When R is further increased, additional bifurcations take place, but the structure which develops, essentially chaotic flow resulting from a Feigenbaum cascade or a quasi-periodic flow, depends on the amplitude of oscillation. The flow in the different regimes is investigated by a combination of asymptotic and numerical methods. In the small-amplitude high-Reynolds-number limit we show that the flow structure develops on two time scales with chaos occurring on the longer time scale. The chaos in that case is shown to be associated with the unsteady breakdown of a steady streaming flow. The chaotic flows which we describe are of particular interest because they correspond to Navier–Stokes solutions of stagnation-point form. These flows are relevant to a wide variety of flows of practical importance.

1. Introduction

Our concern is with the flow in a squeeze bearing driven by the time-dependent motion of one of the walls bounding the fluid. We restrict our attention to the case when the wall moves periodically in time; this simplifies the stability and bifurcation problems associated with the flow since Floquet theory gives a natural definition of instability for the flow. We note that, except for slowly varying flows, the concept of instability for an unsteady flow is not well understood.

The flow which we investigate depends on two spatial variables and time. However, the flow is a Navier–Stokes solution of the stagnation-point type so that one spatial variable may be removed from the problem. The flow is characterized by the Reynolds number R and Δ, the non-dimensional wall oscillation amplitude. The major simplification of our work is that we assume that the walls bounding the fluid are infinite; this differs from real squeeze bearing flows which of course must occur in a finite geometry. We do not address here the question of how the flow we calculate adjusts in order to accommodate sidewall boundary conditions.

In this paper we will investigate the possibility of instability/chaos in flows which retain the assumed stagnation-point structure. Therefore, vortex or wave disturbances

which might also lead to the breakdown of the unique stable flow which occurs for small enough Reynolds numbers are excluded from our analysis.

In fact, as kindly pointed out to the authors by a referee, Secomb (1978) has considered a closely related problem of the flow in a channel where the walls move in a prescribed manner. His analysis concerns symmetric flows in the limiting case of high- or low-frequency oscillations of the wall. In addition he gives results for arbitrary frequency and small-amplitude oscillations. Thus the overlap with the present paper is slight but we shall of course refer to his paper when our analysis can be related to his work.

Another investigation relevant to the present study is that of Stuart *et al.* (1990) who considered the stability of the flow in a squeeze bearing when the distance between the walls varies in time. They used lubrication theory and were able to find an asymptotic solution to the equations governing the growth of Tollmien–Schlichting waves in what turned out to be Poiseuille flow with amplitude varying slowly in time and space. However the method used was unable to describe time-periodic flows. The present investigation began as an attempt to understand the instability of time-periodic squeeze bearing flows to wave or vortex disturbances. We shall see that in fact the flow may break down chaotically as a result of an inherent instability associated with the time dependence. The work which we will carry out on squeeze bearing flows is directly relevant to lubrication technology. We will be able to identify the size of external vibrations which a squeeze bearing flow can support before it breaks down and becomes chaotic. That is of some importance because the load bearing properties change significantly when transition occurs. For a discussion of this point see Gross (1980).

In the small Reynolds number limit the flow is unique and stable and may be found using a small Reynolds number expansion. At leading order the flow corresponds to plane Poiseuille flow in the horizontal direction with local amplitude varying periodically in time. At higher Reynolds numbers we find that the flow loses stability to a synchronous symmetry-breaking perturbation which bifurcates supercritically from the basic state. This flow then remains stable for a range of Reynolds numbers before it loses stability to a more complicated type of mode. This breakdown depends on the size of Δ, the oscillation amplitude. For sufficiently large Δ we find that the flow follows the Feigenbaum route to chaos whereas at lower Δ the flow becomes quasi-periodic before chaos occurs. Our results for small Δ suggest the possibility of a large-R structure capable of supporting quasi-periodic and chaotic flows; that structure is relevant to the case when thin Stokes layers develop at each wall. At an intermediate value of the oscillation amplitude Δ we typically find that the flow initially becomes quasi-periodic but then locks onto a periodic solution with period 4π. It then is found to become chaotic. The results obtained for small Δ suggest that a new structure emerges in the limit $\Delta \to 0, R \to \infty$. This limit is explored and we show that quasi-periodicity at small Δ occurs as a result of a Hopf bifurcation from a steady streaming flow driven by the wall motion. Subsequently we find the quasi-periodic flow itself breaks down and becomes chaotic as a result of a Feigenbaum cascade.

The procedure adopted in the rest of the paper is as follows. In § 2 we write down the partial differential system which describes time-dependent flows in squeeze bearings and discuss the basic flow which exists in the absence of any bifurcations. In § 3 the symmetry-breaking bifurcation to a flow synchronous with the basic state is investigated. In § 4 we discuss the subsequent breakdown of the symmetry-breaking flow as a result of period-doubling or quasi-periodic bifurcations. In § 5 the simplified structure which occurs in the limit $\Delta \to 0, \Delta^2 R = O(1)$ is described, and finally in § 6 we draw some conclusions.

2. Formulation of the problem and the basic periodic flow

We consider the flow of a viscous fluid of kinematic viscosity v and density ρ, between the rigid walls given by $y = 0, 2bH(nt^*)$, with t^* denoting time. The Reynolds number R is defined by

$$R = \frac{nb^2}{v}. \tag{2.1}$$

If we introduce the variables η and t, given by

$$\eta = \{y/(bH) - 1\}, \quad t = nt^*, \tag{2.2}$$

then, following Stuart *et al.* (1990), we find that the two-dimensional stream function for the flow may be written in the form

$$\Psi = nbx(V(\eta, t) - \dot{H}). \tag{2.3}$$

The function V is then seen to satisfy

$$V_{\eta\eta t} = \mathscr{L}V + \mathscr{N}V, \tag{2.4}$$

$$V(\pm 1, t) = \mp\dot{H}, \quad V_\eta(\pm 1, t) = 0.$$

Here the linear and nonlinear operators $\mathscr{L}$ and $\mathscr{N}$, respectively, are defined by

$$\mathscr{L}V = \frac{1}{H}\{2\dot{H}V_{\eta\eta} + \eta\dot{H}V_{\eta\eta\eta}\} + \frac{1}{RH^2}V_{\eta\eta\eta\eta}, \tag{2.5}$$

$$\mathscr{N}V = \frac{1}{H}\left(VV_{\eta\eta\eta} - V_\eta V_{\eta\eta}\right). \tag{2.6}$$

It is then apparent that the periodic solution of (2.4) associated with a basic periodic state has V as an odd function of η. We will restrict our analysis to the case when H is a periodic function of time. In addition we must impose an initial condition at $t = 0$ if we address the initial value problem, and a periodicity condition in t when the equilibrium state is considered. In the small Reynolds number limit there is a unique stable solution of (2.4), which reduces, at any instant in time, to Poiseuille flow at leading order. Henceforth we shall refer to this periodic state as $V_B(\eta, t)$ and in the low Reynolds number limit it follows directly from (2.4) that

$$V_B = \frac{\dot{H}}{2}\left\{\eta^3 - 3\eta\right\} + O(R) + \cdots. \tag{2.7}$$

Thus we see that the flow is locally of plane Poiseuille form in the horizontal direction, with its direction and strength varying periodically in time. The stability analysis of Stuart *et al.* (1990) was concerned with the possible instability of (2.7) to Tollmien–Schlichting waves. Here we restrict our attention to the stability of V_B to simpler disturbances corresponding to the linearization of (2.4) about $V = V_B$, for example. In order to calculate V_B we must in general solve (2.4) numerically. Since much of our discussion will depend on the scheme we use we shall give the most essential details of it here.

A point of some importance to be noted is that a unidirectional flow driven by a pressure gradient in the x-direction can be superimposed on the flow discussed above without altering the equations we have derived. The unidirectional flow is determined by an equation involving the imposed pressure gradient and the stagnation-point flow; see for example Secomb (1978).

We determine V_B by solving (2.4) subject to an initial condition chosen to be

consistent with the boundary conditions. As can be seen, the problem is parabolic in time and a suitable finite difference scheme is provided by the Crank–Nicholson method. Dividing the domain $-1 \leqslant \eta \leqslant 1$ into N equal intervals (variable grids are easily incorporated) of length $h = 2/N$, so that $\eta_1 = -1$ and $\eta_{N+1} = 1$, the objective is to obtain a numerical approximation of $V(\eta_i, t_m) = V_i^m$ where $t_m = m\Delta t$, $m = 0, 1, 2, \ldots$, and Δt is the time step.

Spatial discretizations are done by central differences in the usual way and all derivatives are approximated with $O(h^2)$ accuracy. We will use the notation $\mathrm{D}^j V_i^m$ to mean the central difference approximation of $\partial^j V/\partial\eta^j$ at $\eta = \eta_i$, $t = t_m$. For consistency the Neumann boundary conditions are treated to $O(h^2)$ by extending the computational domain to include the fictitious points $\eta_0 = -1 - h$ and $\eta_{N+2} = 1 + h$ with the corresponding dependent values V_0^m and V_{N+2}^m. The no-slip conditions $V_\eta(\pm 1, t) = 0$ give $V_0^m = V_2^m$ and $V_{N+2}^m = V_N^m$. Next, writing second-order finite difference equations at the points η_2 and η_N (see below) yields relations involving V_0^m and V_{N+2}^m which can be eliminated from the equations just found. Spatial discretizations are seen, then, to be of second-order accuracy throughout.

The advantage of using a semi-implicit method such as the Crank–Nicholson scheme rather than a fully implicit one, is that it achieves second-order accuracy in time and space for direct application to linear problems. The discretization of (2.4) takes the form

$$\frac{1}{\Delta t}\left(D^2 V_i^{m+1} - D^2 V_i^m\right) = \tfrac{1}{2}\left(\mathscr{L} V_i^{m+1} + \mathscr{L} V_i^m\right) + \mathscr{N} V_i^m, \tag{2.8}$$

where the right-hand side of (2.8) is the finite-difference approximation of the operators defined above. We note that the nonlinear terms are treated explicitly at this stage and an iteration procedure is described later. The operator $\mathscr{L}$ has time-dependent coefficients depending on the forcing function $H(t)$ but it is easy to show that the discretization of the linear part is $O((\Delta t)^2)$ accurate.

Equation (2.8) holds for $i = 2, \ldots, N$, and together with the boundary conditions provides $(N+1)$ equations for the unknown vector $\boldsymbol{V}^{m+1} = (V_1^{m+1}, \ldots, V_{N+1}^{m+1})^T$ at time t_{m+1} given information at time t_m. In matrix form the system can be written as

$$\boldsymbol{A}\boldsymbol{V}^{m+1} = \boldsymbol{F}_1(\boldsymbol{V}^m) + \boldsymbol{F}_2(\boldsymbol{V}^m), \tag{2.9}$$

where $\boldsymbol{A}$ is an $(N+1)\times(N+1)$ pentadiagonal matrix. The right-hand side is written in two parts: the vector $\boldsymbol{F}_1$ comes from linear terms of the semi-implicit scheme, and the vector $\boldsymbol{F}_2$ contains all the nonlinearities. The inversion of $\boldsymbol{A}$ is easily accomplished by an LU factorization with recursive back substitution. The matrix is diagonally dominant as h decreases and so the inversion is stable.

To maintain second-order accuracy throughout the discretization, a fixed-point iteration is performed to take care of the explicit representation of the nonlinearities in (2.7). This can be achieved by centring the nonlinearities at $t_{m+1/2}$. The following iteration can then used: at the level k we define $\boldsymbol{U}_k = \boldsymbol{V}_k^{m+1}$ and proceed to level $k+1$ by solving

$$\boldsymbol{A}\boldsymbol{U}_{k+1} = \boldsymbol{F}_1(\boldsymbol{V}^m) + \tfrac{1}{2}\boldsymbol{F}_2(\boldsymbol{V}^m) + \tfrac{1}{2}\boldsymbol{F}_2(\boldsymbol{U}_k), \tag{2.10}$$

where $\boldsymbol{U}_0 = \boldsymbol{V}^{m+1}$ obtained by solution of (2.9) at the time level t_{m+1}. The iteration (2.10) updates the nonlinear part of the equation until a convergence criterion is reached. It was found, through numerical experiments, that for the time steps used a single iteration is usually sufficient. We note also that inversion of $\boldsymbol{A}$ in the iteration

procedure is not costly since the LU factorization of $\boldsymbol{A}$ is already known from the $k = 0$ level.

In view of the odd-parity properties of (2.4) about $\eta = 0$ the function V_B may be assumed to be odd about $\eta = 0$, and calculations need only be carried out over one half of the vertical range of interest. We restrict our discussion throughout this paper to the case when

$$H = 1 + \Delta \cos 2t, \quad 0 < \Delta < 1, \tag{2.11}$$

and note that it is sufficiently general to consider a flow of period π since flows of other periods simply correspond to period-π flows at different values of R.

The calculations to determine V_B were carried out on the half-range $0 \leqslant \eta \leqslant 1$ and symmetry conditions imposed. In view of the symmetry of V_B we took $V_B = 0$ at $t = 0$ and marched forward in time until a periodic state was obtained. Figure 1 shows some calculations performed to compute $V_{B\eta\eta}(-1, t)$ for the cases $\Delta = 0.25, 0.45, 0.65$ and $R = 0, 5, 25$. Note that in each of these figures the amplitudes of the oscillations increase with R. We see that our time marching solution of the initial value problem approaches a periodic state, i.e. $V_B(\eta, t)$, for a range of values of R. At higher values of R this is not the case and we shall return to that situation in the following section.

3. The initial symmetry-breaking bifurcation from $V = V_B(\eta, t)$

In order to verify the calculations discussed above we carried out some runs over the whole range of values of η thereby ignoring the symmetry which V_B possesses. We found that at low values of R the two calculations gave the same odd function $V_B(\eta, t)$. However when the Reynolds number increases the symmetry is lost at a critical value of R which we denote by R_s. A detailed discussion of that breakdown is given later, but in order to set the scene we first plot in figure 2 the quantity

$$I(R) = \int_0^{\pi} V^2(0, t)\, \mathrm{d}t, \tag{3.1}$$

for the case $\Delta = 0.45$ and a range of values of R.

It is clear that $I = 0$ when $V = V_B(\eta, t)$ because of the odd parity of the latter function. We see that when $R = R_s$ there is a bifurcation to a solution with $I \neq 0$. This type of breakdown occurs at all values of Δ for sufficiently high values of R. We will discuss the dependence of R_s on Δ later. In all cases, the flow bifurcating from the solution $V = V_B$ was found to be no longer odd in η, but at the same time remains synchronous with the wall motion. The solution which bifurcates at $R = R_s$ was found to be stable for a further range of values of R before itself breaking down in a much more complicated manner.

Figure 3 shows $V_{\eta\eta}(-1, t)$ for the case $\Delta = 0.45, R = 48$, a value just above the symmetry-breaking bifurcation; we note that the bifurcating flow is again synchronous with the wall motion. As mentioned above, calculations at other values of Δ gave the same kind of supercritical bifurcation to a flow synchronous with the forcing. We stress again that this initial breakdown is always associated with a loss of symmetry of the fluid motion about the $\eta = 0$ plane.

We also note the symmetry-breaking solution is not unique and a given non-symmetric periodic solution may be used to generate another one by changing $\eta \to -\eta$ and the sign of V. The question of which solution is attained numerically is determined by the errors associated with the numerical scheme. Later we shall examine

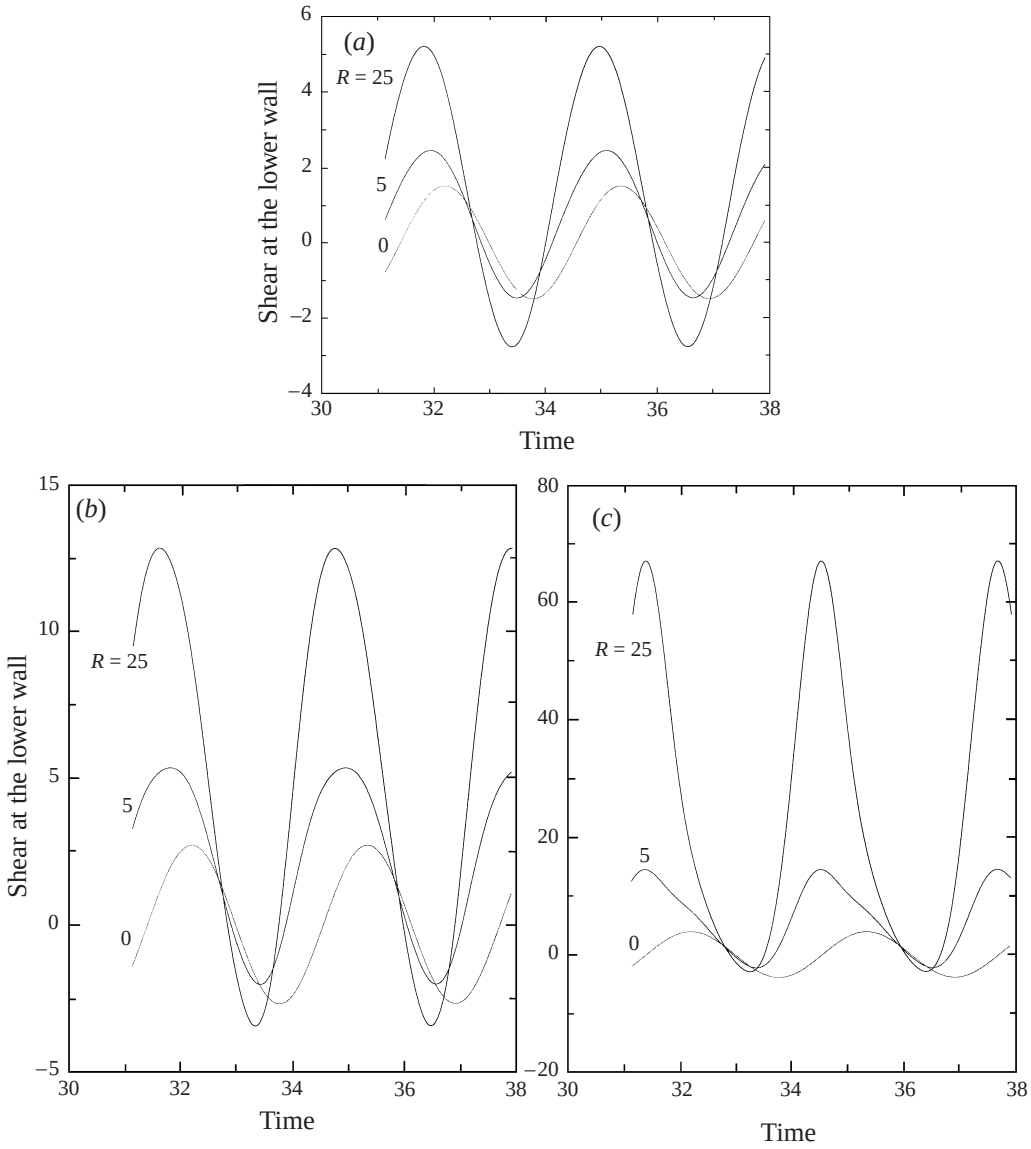

FIGURE 1. The wall shear $V_{B\eta\eta}(-1,t)$ for $R = 0, 5, 25$, and (*a*) $\Delta = 0.25$, (*b*) $\Delta = 0.45$, (*c*) $\Delta = 0.65$.

in some detail the asymptotic small-amplitude structure of the symmetry-breaking bifurcation at $R = R_s$.

At sufficiently small values of the Reynolds number R, the only solution of (2.4) is the basic periodic state $V = V_B(\eta, t)$. Suppose that this solution is perturbed by writing

$$V = V_B + \hat{V}(\eta, t)$$

where $|\hat{V}| \ll |V_B|$. The linearized differential equation satisfied by $\hat{V}$ is found to be

$$\hat{V}_{\eta\eta t} = \mathscr{L}\hat{V} + \frac{1}{H}\{V_B\hat{V}_{\eta\eta\eta} + \hat{V}V_{B\eta\eta\eta} - V_{B\eta}\hat{V}_{\eta\eta} - V_{B\eta\eta}\hat{V}_{\eta}\}. \tag{3.2}$$

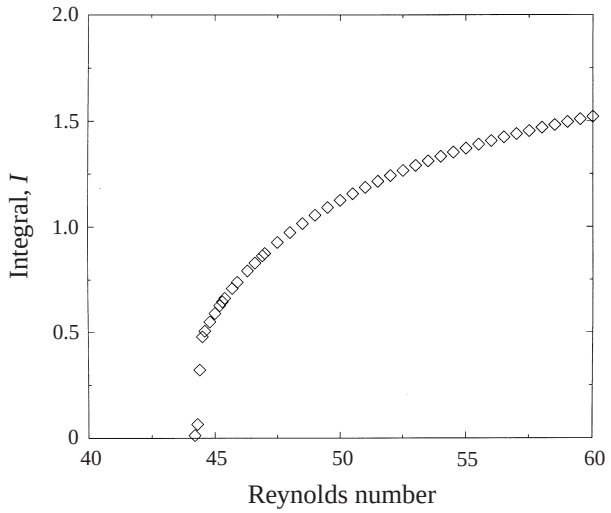

FIGURE 2. The integral I defined by (2.12) for the case $\Delta = 0.45$.

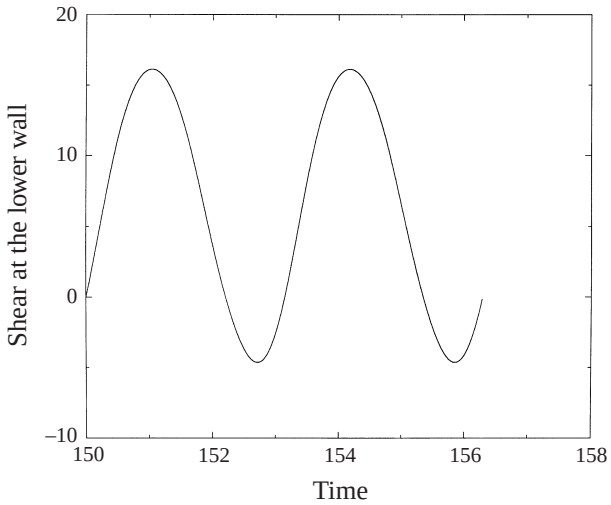

FIGURE 3. The function $V_{\eta\eta}(-1, t)$ for the case $\Delta = 0.45$ and $R = 48$.

The perturbed stream function $\hat{V}$ can be either odd or even about $\eta = 0$. We found numerically that the most unstable perturbations are even about $\eta = 0$ and the appropriate conditions on (3.2) are

$$\left.\begin{aligned} \hat{V} = \hat{V}_\eta = 0, \quad & \eta = 1, \\ \hat{V}_\eta = \hat{V}_{\eta\eta\eta} = 0, \quad & \eta = 0. \end{aligned}\right\} \tag{3.3}$$

The coefficients in (3.2) are periodic in t with period π so that, on the basis of Floquet theory, we expect that $\hat{V}$ can be written in the form

$$\hat{V} = \mathrm{e}^{\mu t} V^+(\eta, t), \quad V^+(\eta, t + \pi) = V^+(\eta, t), \tag{3.4}$$

where μ, the Floquet exponent, will in general be complex. Similar eigenvalue problems have been solved by for example Hall (1978). In that paper a value of μ was found by

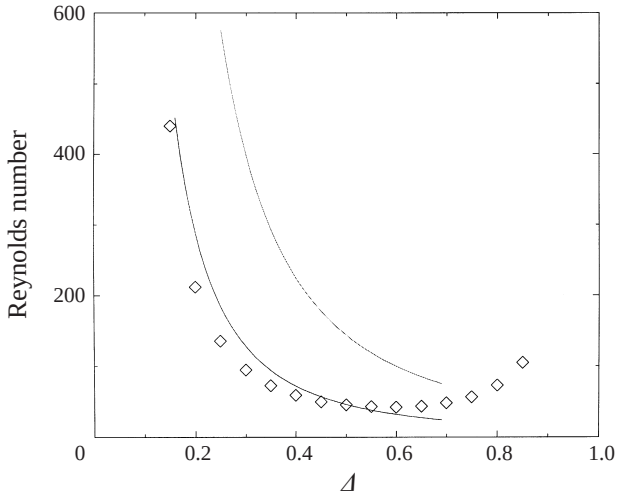

FIGURE 4. The diamonds correspond to the boundary between stability and instability of the flow V_B. The lower curve corresponds to the small-Δ predictions of this boundary and the upper curve corresponds to the onset of quasi-periodicity.

Fourier expanding the disturbance function corresponding to V^+ thereby converting the disturbance partial differential system into an infinite set of coupled ordinary differential equations. The value of μ may then be found from the solution of a truncated form of that set of equations. Here we shall use the efficient approach utilizing the unsteady code rather than solving eigenvalue problems, and compute the value of μ with the largest real part by a direct forward integration of the initial value problem for $\hat{V}$. The drawback of this approach is that it identifies only the most unstable mode; this, however, is sufficient for our purposes here.

We computed μ by integrating (3.2) subject to (3.3) and an appropriate (essentially arbitrary) initial condition on $\hat{V}$. The equation was marched forward and μ estimated by the comparison of the values of some flow quantity over time intervals of length π, until a converged value was found. The number of periods over which it was necessary to integrate the linearized equations to find μ was found to be dependent on Δ and R though in no case was it required to integrate over more than 50 periods. The value of R at which $\mu_r = 0$ is denoted by $R = R_s$ and corresponds to the boundary between the regions where $V_B(\eta, t)$ is stable and unstable to symmetry-breaking perturbations respectively. In figure 4 the diamond symbols show R_s as a function of Δ. First, we should point out that in addition to symmetry-breaking perturbations there exist unstable modes with $\hat{V}$ odd in η but these are stable until much higher values of R. Also shown in figure 6 are two curves derived on the basis of the limit $\Delta \to 0$, $R \to \infty$ analysed later. The lower of the two curves is an asymptotic approximation to the boundary denoted by diamonds.

Figure 4 shows that at any value of Δ the flow corresponding to $V_B(\eta, t)$ loses symmetry about $\eta = 0$ when $R > R_s(\Delta)$. The results suggest that there is a loss of symmetry for $\Delta \to 0$ with $R \to \infty$; in fact the calculations suggest the distinguished limit $\Delta \to 0, R_s = O(\Delta)^{-2}$ as the form of figure 4 when Δ is small. We have plotted results only for $\Delta \leqslant 0.85$ since that is probably above the limit of the physical relevance of our results considering that when $\Delta = 1$ the walls touch. Note also that the Floquet exponent was found to be always real within the vicinity of the curve

of figure 4. Following a comparison between figure 2 and figure 4 there seems little doubt that the linearized instability discussed above is responsible for the bifurcations found in the numerical solution of the full partial differential system. The fact that the Floquet exponent of the linear theory is real is again consistent with the synchronous nature of the bifurcation. Before further discussion of the breakdown which occurs at even higher Reynolds numbers, we describe the form of the bifurcation at the first breakdown Reynolds number R_s.

3.1. *The small-amplitude solution in the neighbourhood of* $R = R_s$

It is a routine multiple scale analysis to determine an evolution equation for the amplitude of the symmetry-breaking disturbance. Therefore we will give only the essential details of the expansion procedure here. We first write

$$R = R_s + \epsilon^2 \hat{R} + \cdots,$$

with $0 < \epsilon \ll 1$ and define a small time scale T by

$$T = \epsilon^2 t.$$

An asymptotic solution of (2.4) is then sought in the form

$$V = V_B(\eta, t) + \epsilon A(T)\, \hat{V}(\eta, t) + \cdots .$$

Here $\hat{V}$ is the neutral eigenfunction corresponding to $\mu = 0$ at $R = R_s$ whilst $A(T)$ is the amplitude of the disturbance. The $O(\epsilon^2)$ system is found to have a solution for any A but, in the usual manner, the $O(\epsilon^3)$ system requires an orthogonality condition to be satisfied if it is to have a solution. This condition takes the form

$$\frac{\mathrm{d}A}{\mathrm{d}T} = a_1 \hat{R} A + a_2 A^3, \tag{3.5}$$

where a_1 and a_2 may be written down in terms of integrals involving the orders ϵ and ϵ^2 disturbance fields. In fact $a_1 > 0$ since the flow is stable for $\hat{R} < 0$ and the sign of a_2 can only be found by evaluation of the integrals which define a_1 and a_2. The results of figure 2 indicate that $a_2 < 0$ so that (3.5) describes a supercritical bifurcation to a finite-amplitude perturbation superimposed on the basic state $V = V_B(\eta, t)$.

4. The subsequent development of the bifurcating periodic solutions

Here we shall discuss in some detail the results obtained at values of the Reynolds number significantly beyond R_s. More details of the methods described below can be found in numerous books and articles. We mention the book by Bergé, Pomeau & Vidal (1984) and the review article by Eckmann & Ruelle (1985). For an application of such methods to data extracted from an experimental investigation of a chemical reaction, see, for example, Roux, Simoyi & Swinney (1983).

The field $V(\eta, t)$ is known numerically at discrete points in space and time from the numerical procedure described earlier. Physically $-V + \dot{H}$ is the dimensionless vertical velocity at a given point, and given a fixed level $\eta = \eta_0$ the time series $V_0(t) = V(\eta_0, t) - \dot{H}(t)$ can be constructed. This time series can be used to classify the dynamics. For instance, if the forcing function is harmonic of the form

$$H(t) = 1 + \Delta \cos(2t), \qquad 0 < \Delta < 1,$$

and the dynamics locks onto the driving frequency, then $V_0(t)$ is a periodic function of period $T = \pi$. All maxima of $V_0(t)$ are then equal and separated by a time π, the same

being true for the minima. (Note that maxima/minima of $V_0(t)$ can be thought of as the Poincaré sections of the phase plane $\left(V_0, V_0'\right)$ at the points where $V_0' = 0$ and V_0'' is less/greater than zero, respectively.) With $V_0(t)$ known (the sampling is no smaller than the numerical time step Δt) the following are computed: (i) the critical points (minima and maxima), (ii) the discrete Fourier transform giving the spectral energy of the signal, (iii) the return maps of minima and/or maxima. The critical points are estimated by following $V_0(t)$ at the time intervals Δt and performing a quadratic polynomial fit, whenever the discrete function changes monotonicity, to estimate more accurately both the value of a critical point and its position in time. Unless stated otherwise, the signals used to produce the graphs in this paper are obtained from $V_0(t) = V(-0.5, t) - \dot{H}(t)$. Return maps are useful in characterizations of chaotic or quasi-periodic attractors. Briefly, if the minima of $V_0(t)$ are denoted by $\{m_i\}_{i=1}^{\infty}$, the return map is the object in the plane obtained from the points $(m_i, m_{i+1})_{i=1}^{\infty}$. As an example, given a series of iterates $\{m_i\}_{i=1}^{\infty}$ generated from the well-known logistic map, the return map gives points lying on the parabola characteristic of the map. In more complex dynamical systems like the partial differential equation studied here, the return map can produce much more complicated objects including folding and self-similarity (see later). (For related results from computational studies of the Kuramoto–Sivashinsky and related systems see Papageorgiou & Smyrlis 1996; Smyrlis & Papageorgiou 1991.)

In addition to the critical points of $V_0(t)$ and their return map, we can also project the infinite-dimensional dynamics onto three-dimensional trajectories. A three-dimensional vector $\boldsymbol{x}(t)$ is constructed in one of two ways: (i) $\boldsymbol{x}_1(t) = (V_0(t - 2\tau), V_0(t-\tau), V_0(t))$, where $\tau > 0$ is a given delay, and (ii) $\boldsymbol{x}_2(t) = (V_0(\eta_1, t), V_0(\eta_2, t), V_0(\eta_3, t))$, where η_1, η_2, η_3 are given points inside the channel. In the results to be presented here we have taken $\eta_1 = -0.5$, $\eta_2 = 0$, $\eta_3 = 0.5$. Useful diagnostics follow from Poincaré sections of such trajectories with a given plane. (In the results presented here, the Poincaré cross-sections are generated by the trajectory intersections with the plane $x_3 = 0$.) This diagnostic is particularly useful in evaluating quasi-periodic temporal dynamics in conjunction with Fourier transforms. Equivalently phase planes in two dimensions are obtained by constructing the vector $\boldsymbol{x}(t) = (V_0(t - \tau), V_0(t))$. We found in our simulations that the results can be classified essentially by the size of the amplitude Δ. In the first instance we discuss results for sufficiently small values of Δ; more precisely, sufficiently small corresponds to $\Delta \leqslant 0.45$, approximately.

4.1. *Results for relatively small Δ*

In order to illustrate results typical of the small-Δ case we first present results for $\Delta = 0.25$. Here we find that the symmetric state breaks down to a synchronous asymmetric flow when $R_s \approx 135.6$. This synchronous flow remains stable until a Reynolds number of about $R = 544$. The mode which destabilizes the synchronous asymmetric flow has a complex-conjugate pair of eigenvalues crossing into the right half-plane $\mu_r > 0$, where μ again denotes the Floquet exponent. This change in flow structure may be seen in figure 5 where we have shown the Poincaré cross-sections for different values of R with $\Delta = 0.25$. When $R < 544$ the cross-section is a pair of points corresponding to a periodic solution of single frequency. When R is increased a pair of closed curves develops; the flow is then quasi-periodic with frequencies corresponding to the driving frequency and the imaginary part of μ which exists when R passes through 544 (see for example the results in figure 5(a, b) for $R = 560, 600$). When R is increased further to $R = 640$ and 680 shown in figure 5(c, d), the flow remains quasi-periodic with two frequencies even though the Poincaré cross-sections contain

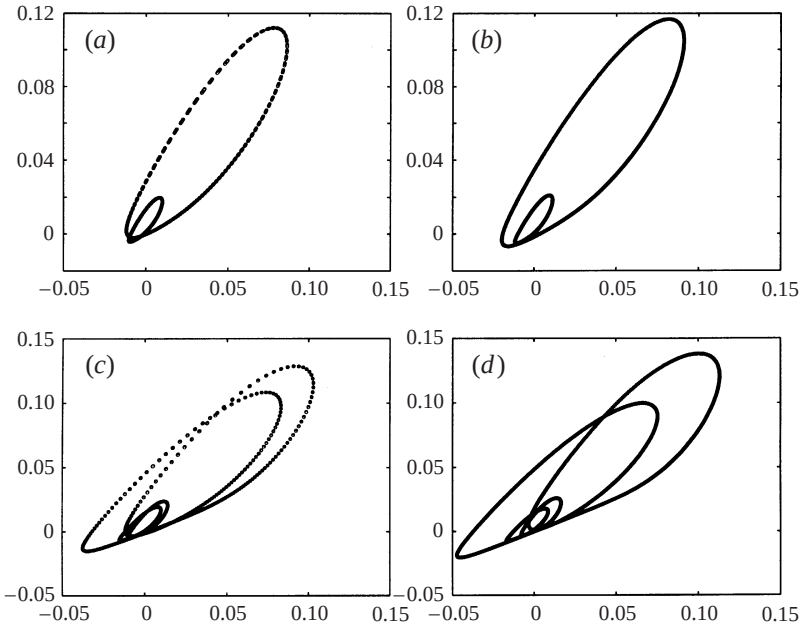

FIGURE 5. Poincaré cross-sections beginning at just above the onset of quasi-periodic flow for $\Delta = 0.25$ and $R = 560, 600, 640, 680$ (*a–d*).

more turns. Parts of the sections overlap and this is the case for the results in figure 6 also.

Figure 6 shows how the cross-sections develop at even higher values of R. At a Reynolds number of 711 we see that the cross-sections appear to have become connected and at a Reynolds number of 1600 two apparently self-similar structures have developed; these structures are enlarged for the sake of clarity. The development of self-similarity suggests that the flow is now chaotic. We note, however, that at even higher values of R the self-similarity is no longer present. In figures 7(*a*) and 7(*b*) we show the velocity time plots and the corresponding frequency spectra for $\Delta = 0.25, R = 711$ and 1600. The dominant response has frequency 2 and is in phase with the driving oscillations. The magnification shows the lower frequencies which enter due to the initial quasi-periodic modulation and subsequent nonlinear interactions. The spectrum at 1600 is not noticeably more 'broad band' than the other so we do not have conclusive evidence of the presence of chaos at $R = 1600$. However we shall be able to make further comments on the possible chaotic structure in this regime in § 5 where the limit $\Delta \to 0$ is considered. Here we merely state that the results found in that section suggest that chaos is indeed present in this regime and is associated with a period-doubling cascade on the second frequency. The value of the smallest frequency present in the spectrum of figure 7(*b*) is about 0.024.

Figure 8 shows how the cross-sections develop at even higher values of R. It is observed that there is no evidence of self-similarity and the flow is most probably quasi-periodic. Our calculations suggest that for large R the second frequency scales like R^{-1}. The relevance, and importance, of this $O\left(R^{-1}\right)$ time scale for $\Delta \ll 1$ will be made clear in the following section. In fact the presence of this longer time scale enables a chaotic structure to develop as a modulation to the fast time variation associated with the forcing from the wall.

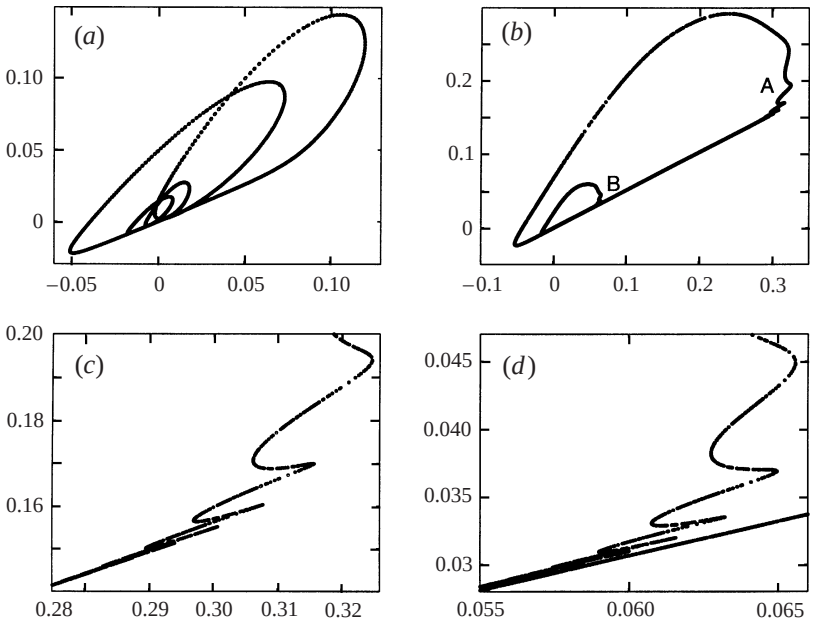

FIGURE 6. Poincaré cross-sections for $\Delta = 0.25$, $R = 711, 1600$ (a, b). The self-similar structures which develop near A and B for $R = 1600$ have been enlarged in (c, d).

The results obtained above were found by integrating the full equations forward in time from $t = 0$ until either an equilibrium state was reached or enough data were available to determine the nature of the flow from, for example, Poincaré cross-sections. In some cases we used data from a completed run at a given value of the Reynolds number to begin a run at a neighbouring value of R. In all such cases we found the dynamics of the flow after a sufficiently long time was indistinguishable from that obtained by beginning the integration with zero flow. We shall see below that this is not the case at larger values of Δ where it appears that several attractors can exist at a given R.

Results similar to those obtained above were found for other values of Δ less than 0.45; some of these results are described in figure 9. The first symmetry-breaking bifurcation is indicated and the flow remains synchronous with the driving frequency until the indicated quasi-periodic bifurcation. In the regimes where self-similar structures are indicated in the figure we believe the flow to be chaotic. In all of the small-Δ cases we were unable to determine from power spectra whether the onset of chaos was caused by period doublings associated with the small frequency leading to the quasi-periodic flow or by the appearance of a third frequency. The difficulty in using the power spectra to settle this issue is apparent in figure 7 where we see that the energy associated with the second frequency is much smaller than that of the driving frequency.

4.2. *Results for relatively large* Δ

The results described next are typical of those obtained for values of Δ bigger than about 0.45. The largest value of Δ studied extensively was 0.65; higher values of Δ are probably of less physical interest, but some results are included in § 3.

We begin by describing results for the relatively large value of $\Delta = 0.65$. Solutions begin by locking onto the driving frequency with $V_0(t)$ being periodic of period $T = \pi$.

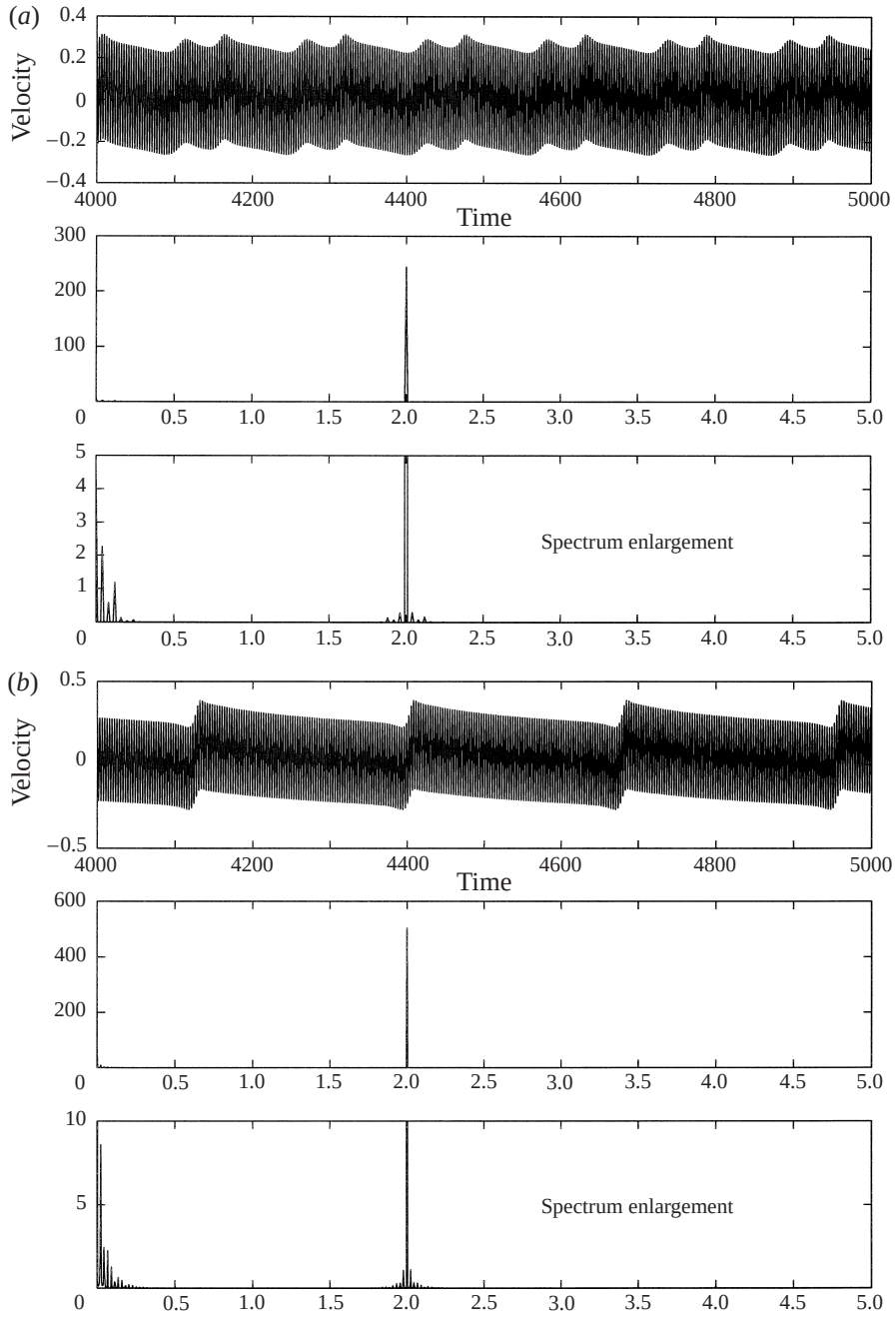

FIGURE 7. The velocity time traces and corresponding frequency spectra of the time signal $V(-1/2, t) - \dot{H}$ as the Reynolds number increases. $\Delta = 0.25$, and (*a*) $R = 711$, (*b*) $R = 1600$.

At a Reynolds number of approximately $R = 60.39 = R_{s2}$ a period doubling in $V_0(t)$ takes place and the period becomes $T = 2\pi$. The synchronous flow which exists for $R < 60.39$ is symmetric about $\eta = 0$ for $R < R_s = 43.77$ where it loses stability to the symmetry-breaking perturbations. Note that since the bifurcation which takes

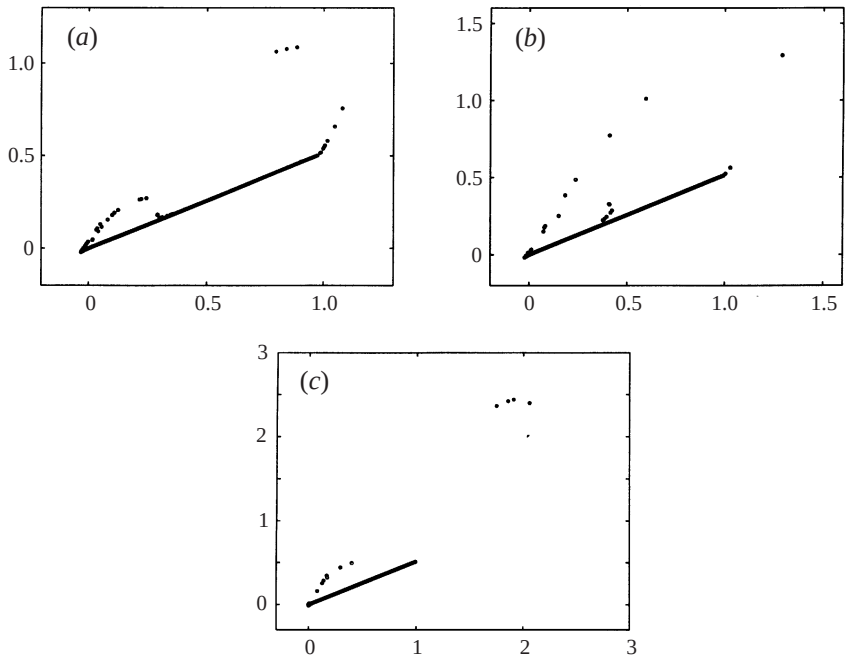

FIGURE 8. Poincaré cross-sections for $\Delta = 0.25$, $R = 5000, 6000, 10\,000$ (*a–c*).

R subwindow	Period T	Subwindow length	Length ratio
$R \leqslant 60.38$	π	60.38	—
$60.39 \leqslant R \leqslant 74.6$	2π	14.21	4.25
$74.605 \leqslant R \leqslant 78.46$	4π	3.855	3.69
$78.465 \leqslant R \leqslant 79.199$	8π	0.734	5.25
$79.2 \leqslant R \leqslant 79.3545$	16π	0.1545	4.75
$79.355 \leqslant R \leqslant 79.3865$	32π	0.0315	4.91
$79.387 \leqslant R \leqslant 79.394$	64π	0.007	4.5
$79.395 \leqslant R \leqslant 79.396$	128π	—	—

TABLE 1. The Feigenbaum cascade for a relatively large value of $\Delta = 0.65$. A period doubling takes place on the basic forcing period π.

place at $R = R_s$ leads to a flow synchronous with the forcing, phase locking occurs for $0 < R < R_{s2}$. In addition, instead of a single maximum and single minimum the signal contains two maxima and two minima after the period doubling. Solutions remain 2π-periodic as the Reynolds number increases until a further period-doubling bifurcation takes place at approximately $R = 74.605$, the solution now being periodic with period $T = 4\pi$ and the signal containing four maxima and four minima. It has been established numerically that a period-doubling route to chaos is dictating the dynamics according to the Feigenbaum scenario (see Feigenbaum 1979, 1980). These results are summarized in table 1 which gives computed window boundaries which support different periodic solutions. In addition the estimated lengths of computed subwindows are also given, as well as the ratio of successive lengths as a period-doubling cascade takes place.

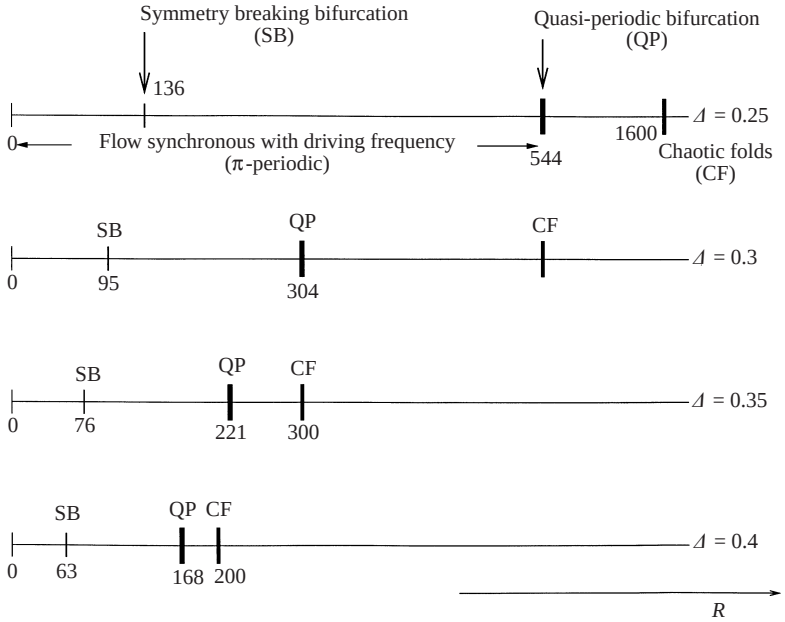

FIGURE 9. Schematic of the dynamics at relatively low values of Δ as the Reynolds number increases. Self-similar chaotic dynamics occur beyond the quasi-periodic bifurcation boundary as indicated.

All results in table 1 were computed with $h = 1/500$ and $\Delta t = 2\pi/25000$. Periodicity of solutions along with the period were found efficiently by inspection of the evolution of the critical points of $V_0(t)$. For instance for the 16π-periodic solutions the minima (or maxima) evolve, after initial transients, to lie on 16 straight lines with successive minima on each line separated by a time of 16π. We also note that the results shown in table 1 were obtained by marching forward in time from zero initial flow. Identical results are obtained by varying the Reynolds number slightly after equilibrium has been achieved.

It can be seen from the computed values of successive window lengths that our results are consistent with the Feigenbaum universal theory. The theoretical value is 4.6692016..., and agreement is quite reasonable. Agreement can be improved by refining subwindow boundaries, but given the computational expense required by this (convergence to an attractor slows down near boundaries and long runs are required), such an exercise is not pursued further here. There exists an accumulation point at a Reynolds number R_∞, say, which is approximately equal to 79.4 and beyond which the dynamics are chaotic.

At higher values of R the dynamics are mostly chaotic. There are, however, small windows supporting time-periodic solutions: for example solutions with periods 20π at $R = 80$, 3π at $R = 85$, 6π at $R = 86$, with non-periodic motions in between were obtained by marching forward in time from zero flow. Such behaviour is typical just beyond a Feigenbaum route to chaos.

We consider next a value $R = 100$ where the dynamics are chaotic. The time series $V_0(t)$ is constructed by fixing $\eta_0 = -0.5$. This is then used, with a delay $\tau = 500\Delta t$, to obtain the phase plane. The results are presented in figure 10. Both the signal and its phase-plane suggest chaotic dynamics, but additional evidence is given by the evolution of the critical points of $V_0(t)$ together with their corresponding return

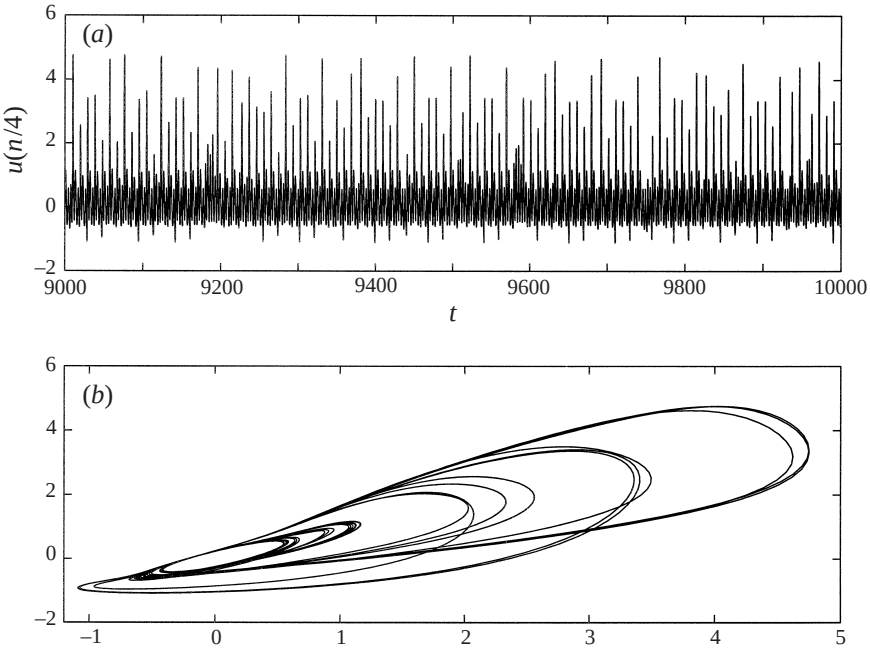

FIGURE 10. The dynamics in the chaotic regime for $\Delta = 0.65$, $R = 100$. (a) Velocity time trace, (b) phase plane.

maps, shown in figure 11. The irregular temporal evolution of the signal is clearly seen in the evolution of the critical points; the return maps, however, show structures in the plane which include foldings characteristic of chaotic dynamics. By analogy with the Hénon map we can surmise that the dimension of such objects is expected to be a number between 1 and 2.

The geometrical nature of the chaotic attractor including foldings is apparent also in the results presented in figure 12, which shows Poincaré sections of the three-dimensional trajectory $\boldsymbol{x}_2(t)$ (see above for the definition), with the plane $x_3 = 0$. Foldings are found and a clearer picture of these is presented by the three enlargements in the neighbourhood of the points A, B and C.

Further calculations were carried out for $\Delta = 0.6, 0.55, 0.5, 0.45$. The results for the three higher values of Δ are similar so we describe in detail only the case $\Delta = 0.6$. We again find that there is a chaotic attractor associated with a period-doubling route from the basic driving period. In addition, however, there is a route to chaos from a period-doubling cascade beginning with period $3\pi \rightarrow 6\pi \rightarrow 12\pi \ldots$. Table 2 indicates the main milestones of the two routes. We see that the '3π' attractor develops into a chaotic flow whilst the 'π' attractor is locked onto a period-2π solution. Furthermore the results shown in table 2 again give predictions for the Feigenbaum constant consistent with the theoretical value. Also notice that the results of table 2 for the period-'π' attractor were found by marching forward in time from an equilibrium state at a nearby value of the Reynolds number since we found that marching forward in time from zero initial flow invariably produced a solution corresponding to the period-3π attractor for R greater than about 79.2. In order to see the origin of the period-3π attractor we followed its evolution numerically as R was decreased. In these calculations the initial data were taken to be those from a previous converged run. We found that the attractor could not be followed below a Reynolds number of about

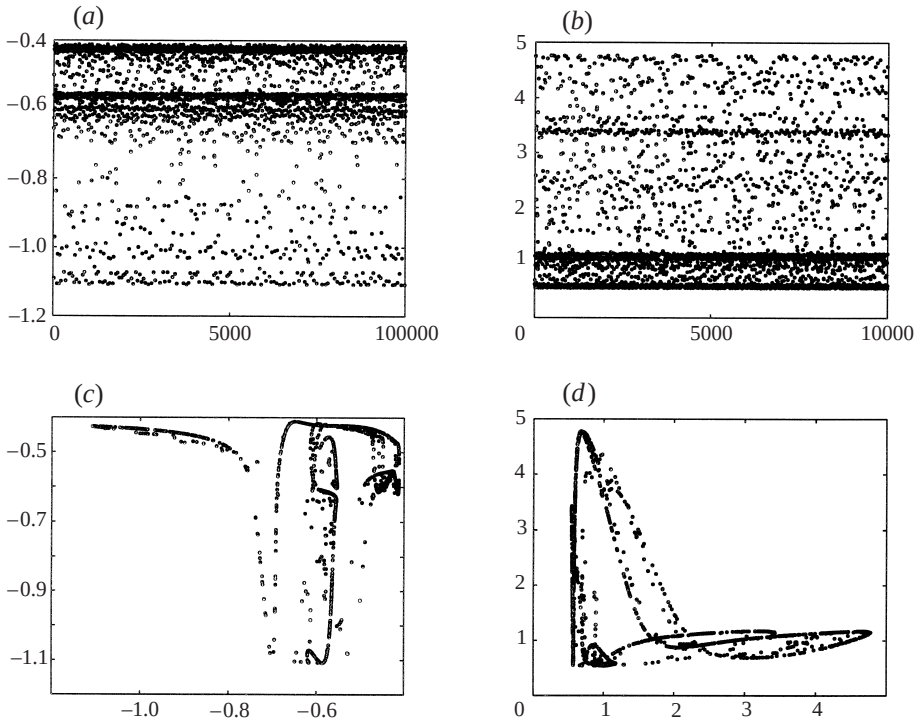

FIGURE 11. The evolution of (*a*) the minima and (*b*) maxima of the velocity signal at $\eta = -\frac{1}{2}$, together with the corresponding return maps (*c*, *d*) in the chaotic regime for $\Delta = 0.65$, $R = 100$.

R subwindow	Period T	Subwindow length	Length ratio
$R \leqslant 71.0$	π	71.0	—
$71.5 \geqslant R \leqslant 85.09875$	2π	13.59875	5.22
$85.099 \geqslant R \leqslant 87.6775$	4π	2.5785	5.28
$87.6778 \geqslant R \leqslant 87.977$	8π	0.2992	8.62
$79.196 \leqslant R \leqslant 80.736875$	3π	—	—
$80.737 \leqslant R \leqslant 81.3449375$	6π	0.6079375	—
$81.345 \leqslant R \leqslant 81.476875$	12π	0.131875	4.61
$81.477 \leqslant R \leqslant 81.50546875$	24π	0.02846875	4.63
$81.505625 \leqslant R \leqslant 81.5116125$	48π	0.0059875	4.76
$81.511625 \leqslant R \leqslant 81.51275$	96π	0.001125	5.32
$R = 81.513$	192π	—	—

TABLE 2. Computed periodic solutions for $\Delta = 0.45$. Period doublings are found starting from π and 3π periodic solutions with the two attractors partly co-existing. The results indicate that the Feigenbaum scenario is at play.

79.196, below which the period-2π solution was obtained. This value of R denotes a limit point and a linear stability of the 3π-solutions as R decreases yields an eigenvalue passing through zero, confirming this structure. The two cascades are shown in figures 13(*a*) and 13(*b*). The figures show the minima of the signal $V_0(t) = V(-0.5, t) - \dot{H}$ after

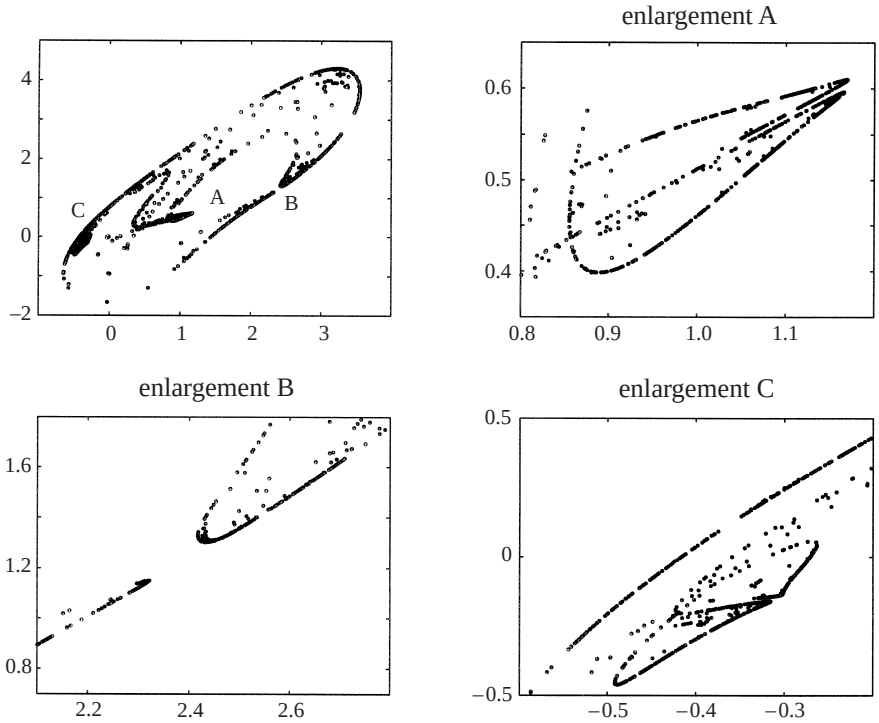

FIGURE 12. Poincaré cross-section for the case $\Delta = 0.65$, $R = 100$ obtained from the intersection of the trajectory $(x_1(t), x_2(t), x_3(t))$ with the plane $x_3 = 0$.

transients have died out, starting from $R = 0$. Figure 13(a) includes the continuation of the unstable symmetric branch beyond the symmetry-breaking bifurcation. The cascade on the 3π basic periodic solution is shown in figure 13(b). As R decreases below about 79.196, the 3π-solutions disappear: this point is a limit point with stable and unstable 3π-branches co-existing above this point. The unstable branches are not shown in the figure since they are not obtainable by the present numerical methods. (As mentioned earlier this has been confirmed by a linear stability of the solutions as R decreases towards the limit point.) As R increases a Feigenbaum period-doubling cascade occurs; this, as well as the period-doubling cascade on the 2π-solutions, are summarized in table 2. We also note that, if symmetry is maintained in the problem, the symmetric branch remains π-periodic until approximately $R = 250$ when the first period-doubling takes place.

Clearly it is possible for other attractors to exist which were not accessible from a zero initial flow marching calculation. However, in the ranges of Reynolds number investigated, that is 0–99, apart from the $\pi, 3\pi$ attractors the most attracting solution set found by marching from zero initial flow was a period 11π solution at $R = 87.9$. This attractor also has a period-doubling sequence and perhaps occurs initially as a periodic state emerging from the remnants of the chaotic form of the period-3π attractor.

4.3. *Results for* $\Delta = 0.45$

This is perhaps the most interesting case and the results we obtained have some similarities with both the $\Delta = 0.25$ and $\Delta = 0.65$ cases. As in the $\Delta = 0.25$ case, the symmetric synchronous mode which bifurcates supercritically at $R = R_s$ loses stability

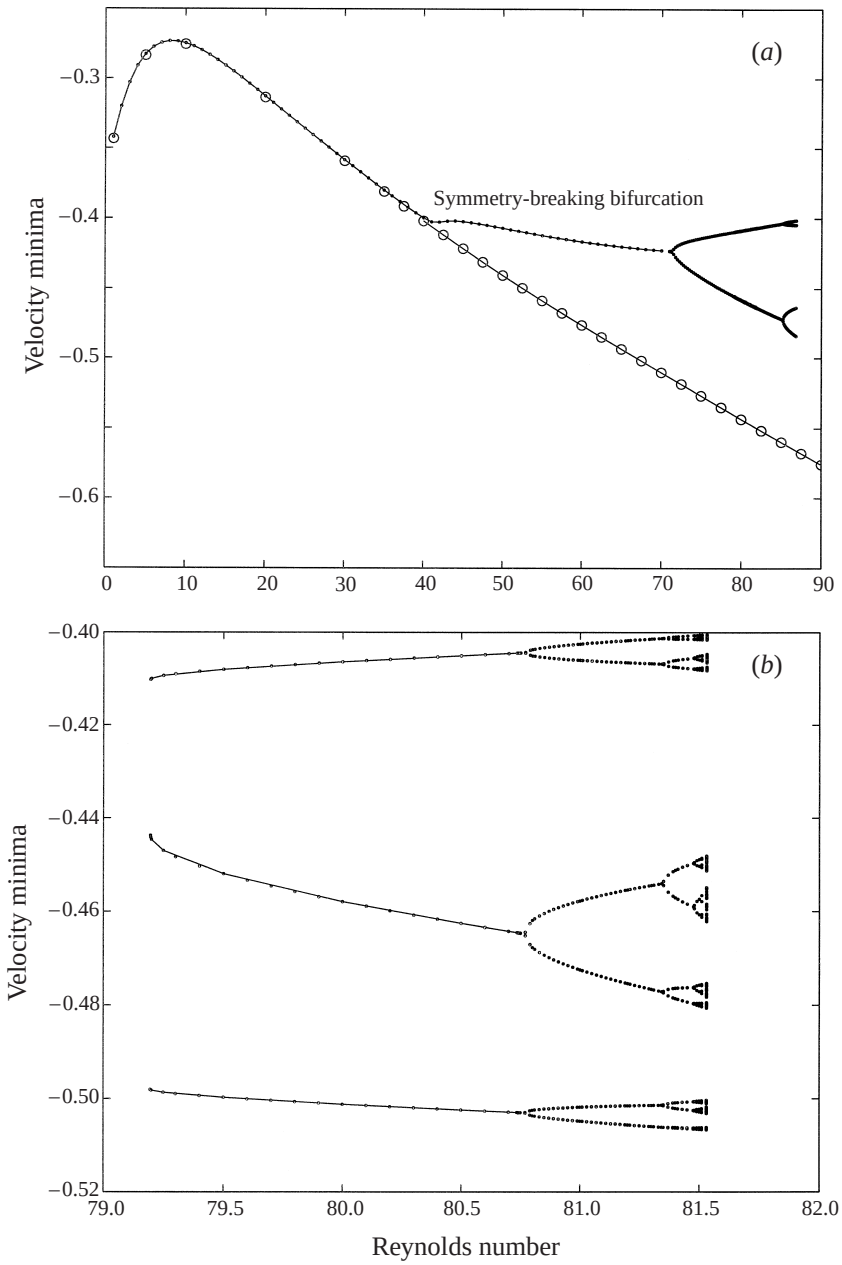

FIGURE 13. Minima of the time signal $V(-1/2, t) - \dot{H}$ as the Reynolds number increases. In (*a*) the circles denote symmetric solutions. (*b*) 3π-basic periodic solution.

as a result of a Hopf bifurcation to a quasi-periodic flow. Figure 14 shows some of the flow properties. The Poincaré cross-section at $R = 136.23$ again has two closed curves typical of the quasi-periodic flows found here. The two frequencies present in the flow are again associated with the driving motion of the wall and the Hopf bifurcation.

However when R is increased further the smaller of the two frequencies approaches

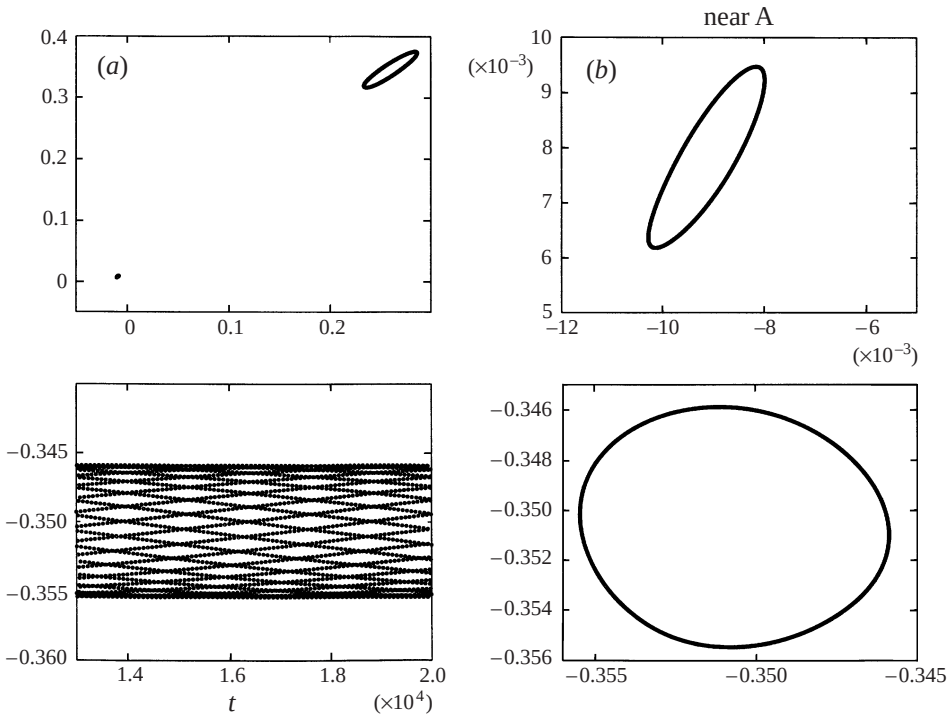

FIGURE 14. Results for the case $\Delta = 0.45$, $R = 136.23$. (a, b) The Poincaré cross-section and an enlargement. The minima of the velocity at $\eta = -\frac{1}{2}$ are also shown (c) along with their return map (d).

$\frac{1}{4}$ of the driving frequency and the flow then locks onto a period-4π solution (i.e. time periodic with period 4π) at approximately the value $R = 136.24$. In our computations based on solutions of the initial value problem starting with a zero initial velocity field, we find that when R increases beyond about $R = 143.9$ instead of locking directly onto a period-4π solution the flow stays chaotic for a considerable interval of time. Figure 15 shows how the interval over which the flow is chaotic increases when R increases. We conclude that for a value of R not too far beyond $R = 143.93$ the large time solution of the initial value problem addressed here is attracted to a chaotic solution. Figure 16 shows additional results for $R = 143.93$: the return map of the minima of $V_0(t)$ is depicted, clearly showing the transient chaotic state and the manner in which the period-4π solution emerges from the chaotic attractor. The numbers on the figure show the four points comprising the return map which correspond to the period-4π solution.

It can be concluded, therefore, that the period-4π solution becomes unstable (at least within the frame of the initial value problem considered in most of this study) and is replaced by a chaotic attractor. We note that such large time behaviour is consistent with physical situations where an experiment would begin with the plate oscillating and the fluid being stagnant at $t = 0$. It is interesting, however, to follow the period-4π solutions by choosing appropriate initial conditions and by taking small increments in the Reynolds number. This enables continuation of the period-4π branch to values of R that would otherwise produce chaotic dynamics. This process was successful for a range of Reynolds numbers and the results are shown in figure 17. We note that for values of the Reynolds number beyond about 148, the increment

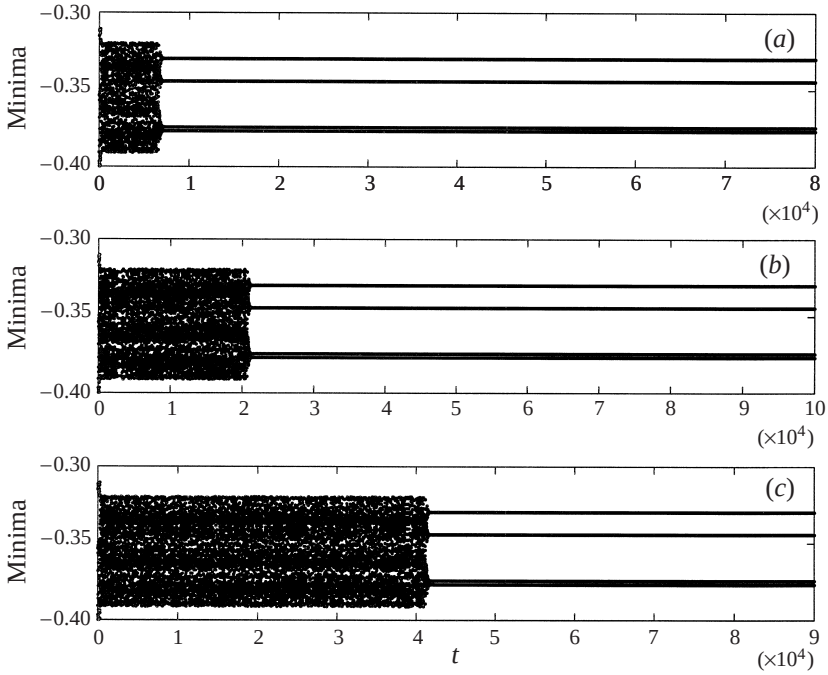

FIGURE 15. Velocity time traces for $\Delta = 0.45$ and different values of R: (*a*) 143.91, (*b*) 143.92, (*c*) 143.93.

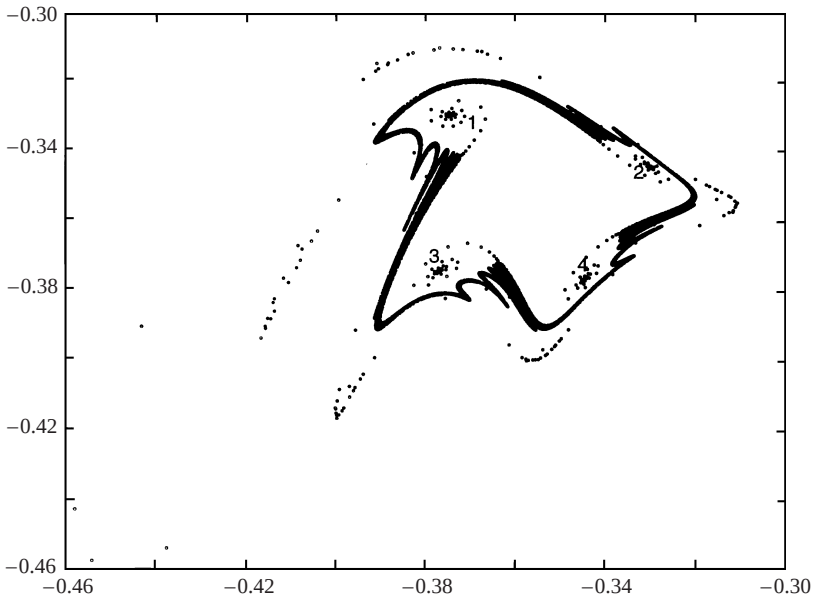

FIGURE 16. The Poincaré cross-section for $\Delta = 0.45$, $R = 143.93$ indicating the emergence of a period-4π solution after a long-lived chaotic transient. The numbers are the four minima after the chaotic transient.

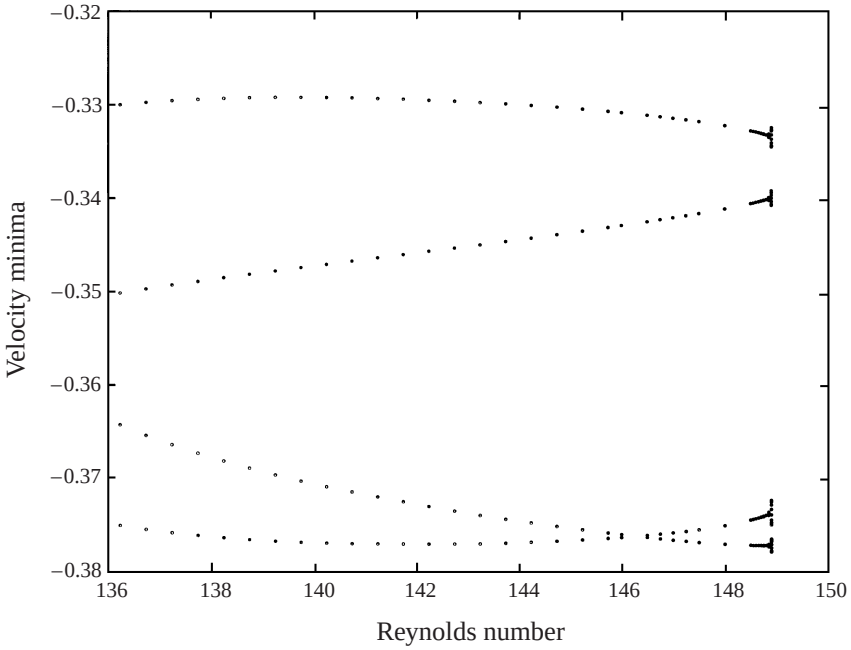

FIGURE 17. Minima of the velocity time trace depicting the period-4π solution. $\Delta = 0.45$.

in the Reynolds number had to be very small and the computations became very costly. Larger steps in Reynolds number were made possible by computing with a Reynolds number of, for example, $R = R_0 + \delta R(\tanh(\alpha t))$, where R_0 is the Reynolds number at which the solution is already known and has converged to a period-4π solution, δR is the increment, and α is a parameter which is usually less than unity; the time-dependence ensures a smoother transition than the usual jump in R by δR. The solutions beyond $R = 148.9$ failed to converge to period-4π solutions and instead locked onto chaotic attractors. In addition, there are other periodic solutions present beyond $R = 149$ such as period-6 solutions. As can be seen from the figure, the lower two branches get very close together at about $R = 146.2$ before opening up again. Note that it is not possible to go from a period-4π solution to a period-3π one smoothly.

The coexistence of chaotic and periodic attractors and the fact that the chaotic ones are more strongly attracting poses considerable difficulty in the construction of weakly attracting periodic solutions. An illustration of the chaotic attractor obtained at $R = 148.75$ is shown in figure 18. Note that a period-4π solution coexists at this value of R as shown in figure 17. The chaotic dynamics depicted in the Poincaré section in figure 18 contain a striking self-similarity. This is clearly shown in the enlargement included in the figure of the small island just below the main highly folded island. As noted previously, by analogy with the Hénon map the dimension of the total object is expected to be a number between 1 and 2.

5. A simplified structure valid in the limit $R \to \infty, \Delta = O(R^{-1/2})$

The results obtained in the last section suggest that for $\Delta \to 0$ there might be an asymptotic structure emerging in the high Reynolds number limit. We shall show next that the results found previously for the smaller values of Δ are in fact in close

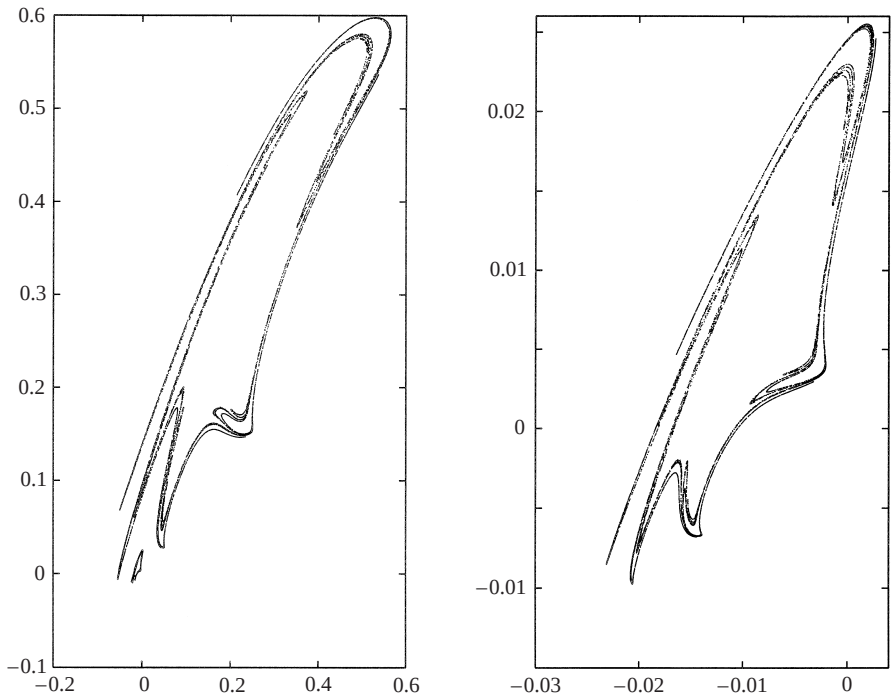

FIGURE 18. The Poincaré cross-section for $\Delta = 0.45$, $R = 148.75$. The graph on the right is an enlargement of the small island labelled A on the left, showing self-similarity of the attractor.

agreement with a simplified asymptotic model of the full problem in which $R \to \infty$ with $R^{1/2}\Delta$ held fixed.

First it is convenient for us to transform (2.4) to a more suitable form by writing

$$V = -\eta\dot{H} + H^3\psi(\eta, t), \tag{5.1}$$

so that ψ is now determined by the partial differential system

$$\psi_{\eta\eta t} = \frac{1}{RH^2}\psi_{\eta\eta\eta\eta} + H^2\left\{\psi\psi_{\eta\eta\eta} - \psi_\eta\psi_{\eta\eta}\right\}, \tag{5.2}$$

$$\psi = 0,\ \eta = \pm 1, \quad \psi_\eta = \frac{\dot{H}}{H^3}, \quad \eta = \pm 1.$$

Notice that (5.2) shows that ψ depends on H only through H^2 and that a basic antisymmetric solution of the system is possible. We shall follow the notation of § 3 and refer to this solution as $\psi = \psi_B(\eta, t)$ since this is the unique stable solution for R sufficiently small. In fact, Secomb (1978) discussed the steady streaming problem in the small-amplitude limit; therefore we shall give here only the essential details of the calculation and refer the reader to that paper. The major difference in our analysis is that we allow the streaming flow to evolve on a long time scale and impose no symmetry on the flow. It is of course essential to allow for this time dependence if we are to determine the cause of the chaos discussed in the previous section.

In the limit of large R, the dominant balance of the linear terms in (5.2) has $\partial^3/\partial\eta^2\partial t \sim \partial^4/R\partial\eta^4$ if $\partial/\partial\eta \sim O(R^{1/2})$ so that boundary layers of thickness $R^{-1/2}$ must exist at the upper and lower walls. Thus for example near the upper wall $\eta = 1$

we define the variable ζ by writing

$$\zeta = R^{1/2}\{1-\eta\}. \tag{5.3}$$

The nonlinear terms in the partial differential equation to determine ψ in the wall layer are then comparable with the linear terms if $\psi \sim O\left(R^{-1/2}\right)$. This is the appropriate wall layer structure for the limit $R \to \infty, \Delta = O(1)$. Here we have made the further assumption that $\Delta = O\left(R^{-1/2}\right)$; this reduces ψ to being of order R^{-1} in the wall layer so the required expansion is

$$\psi = \frac{1}{R}\psi_0(\zeta,t) + \frac{1}{R^{3/2}}\psi_1(\zeta,t) + \frac{1}{R^{3/2}}\psi_M(\zeta) + O\left(1/R^2\right). \tag{5.4}$$

We write

$$\Delta = \frac{d}{R^{1/2}}, \tag{5.5}$$

and ψ_0 is then found from the leading-order approximation to (5.2) in the upper wall layer. We obtain

$$\psi_0 = \frac{\mathrm{i}d}{1+\mathrm{i}}\{\mathrm{e}^{-\zeta(1+\mathrm{i})} - 1\}\mathrm{e}^{2\mathrm{i}t} + \text{c.c.}, \tag{5.6}$$

where c.c. denotes complex conjugate. We note that we have split the order-$R^{-3/2}$ terms into a time-periodic part, ψ_1, and ψ_M which is essentially a steady streaming flow induced by the Reynolds stresses in the upper layer. We find that

$$\frac{\psi_M}{d^2} = \left[\frac{1+\mathrm{i}}{2}\mathrm{e}^{-\zeta(1+\mathrm{i})} + \frac{1+\mathrm{i}}{4}\mathrm{e}^{-\zeta(1-\mathrm{i})}\right] + \text{c.c.} + \frac{\mathrm{e}^{-2\zeta}}{4} + \frac{N\zeta + M}{d^2},$$

and to satisfy no slip at $\zeta = 0$ we have that

$$N = \tfrac{3}{2}d^2,$$

so that for large ζ, $\psi_M \sim \frac{3}{2}d^2(\zeta)$.

This means that the mean part of the flow in (5.4) becomes comparable with the leading-order unsteady form at the edge of the boundary layer, i.e. when $\zeta = O\left(R^{1/2}\right)$. Hence, in the core region $-1 < \eta < 1$, we expand ψ in the form

$$\psi = \frac{1}{R}\overline{\psi}_0(\eta,t) + \frac{1}{R}\phi(\eta) + O\left(\frac{1}{R^{3/2}}\right). \tag{5.7}$$

The leading-order approximation to the equations governing the time-periodic flow (with mean zero) in the core then yields

$$\overline{\psi}_0 = A(t)\eta + B(t),$$

where A and B are found by matching with the wall layers but are in fact not needed here. It is convenient to allow for a slow modulational time scale in the core so we write

$$\tau = \frac{1}{R}t,$$

and allow ϕ in (5.7) to depend on η and τ. We find that ϕ satisfies

$$\phi_{\eta\eta\tau} = \phi_{\eta\eta\eta\eta} + \phi\phi_{\eta\eta\eta} - \phi_\eta\phi_{\eta\eta}. \tag{5.8}$$

In the terminology of steady streaming problems, see for example Stuart (1966), we have chosen scalings such that the outer steady streaming layer entirely fills the channel. From the form of ψ in the wall layer when $\zeta \to \infty$, and a similar analysis

near $\zeta = -1$, we can show that the boundary conditions to be imposed on ϕ take the form

$$\left.\begin{aligned} \phi &= 0, & \eta &= \pm 1, \\ \phi_\eta &= -\tfrac{3}{2}d^2, & \eta &= \pm 1. \end{aligned}\right\} \tag{5.9}$$

Thus (5.8) and (5.9) constitute a self-contained steady-streaming problem for ϕ driven by the Reynolds stresses in the wall layers. In fact by making the transformation $\phi \to \frac{3}{2}d^2\hat{\phi},\ \tau = \left(\frac{3}{2}d^2\right)^{-1}\hat{\tau}$ we may write the problem for $\hat{\phi}$ as

$$\hat{\phi}_{\eta\eta\hat{\tau}} = \frac{1}{R_s}\hat{\phi}_{\eta\eta\eta\eta} + \hat{\phi}\hat{\phi}_{\eta\eta\eta} - \hat{\phi}_\eta\hat{\phi}_{\eta\eta}, \quad \hat{\phi} = 0,\ \hat{\phi}_\eta = -1,\ \eta = \pm 1. \tag{5.10}$$

Here $R_s = \frac{3}{2}d^2$ is to be interpreted as a steady-streaming Reynolds number, see Stuart (1966). Thus the problem for $\hat{\phi}$ is essentially the same as the original forced problem for V except that now the forcing from the walls is purely steady. The system (5.10) does of course allow a solution which is odd about the centre of the channel. An investigation of the steady symmetric problem was made by Secomb whilst Brady & Acrivos (1981) discussed the same problem but with the streaming Reynolds number negative. Such flows are relevant to motions induced by bubbles. After this paper was submitted we became aware of an investigation of (5.10) by Watson *et al.* (1990). (Note, however, that because of the slightly different formulations used the streaming Reynolds number is the negative of the Reynolds number of their paper.) In fact the results we obtained are in good agreement with Watson *et al.* Since our results were obtained with the code used to determine the results of the previous section, we therefore have an independent check on our numerical work.

Now let us discuss the properties of (5.8) and (5.9) and show how the dynamics for ϕ explain some of the numerical results obtained for $\Delta = 0.25$. The first point to note is that (5.8) and (5.9) can support a solution with $\phi = \phi_B(\eta)$ an odd function of η and independent of time. This solution is the appropriate asymptotic approximation to the mean part of $\psi_B(\eta, t)$. In fact for small values of d it can be seen from (5.8) and (5.9) that ϕ takes the form

$$\phi_B = \tfrac{3}{4}d^2\left\{\eta - \eta^3\right\} + O\left(d^4\right). \tag{5.11}$$

At order-one values of d the solution must be calculated numerically. The linear stability of this flow may be found by perturbing about the steady state and marching the linearized form of (5.8) and (5.9) forward in time until the instantaneous growth rate equilibrates. Such a calculation shows that ϕ_B loses stability to a single mode with purely real eigenvalue and having even symmetry about $\eta = 0$. This occurs when $d = 3.39$ so that for small Δ, large R we predict the form of figure 4 for $\Delta \ll 1$ to be

$$R = \frac{(3.39)^2}{\Delta^2} + \cdots .$$

This asymptotic prediction is shown in figure 4 and we see that it is consistent with the $\Delta = O(1)$ calculation for small Δ. The corresponding value d from Watson *et al.* is 3.40.

The linear stability of the steady symmetry-breaking solutions may be checked by a similar linear stability calculation. We find that when $d = 5.99$ (compared to 6.09 from Watson *et al.*) a complex conjugate pair of eigenvalues move into the right half-plane so that a Hopf bifurcation to a periodic state occurs at this value of d. Note again that this flow is periodic on an $O(R)$ time scale quite different from that

R subwindow	Period T	Subwindow length	Length ratio
$d < 5.99(6.09)$	steady	5.19	—
$5.99 < d < 7.0245(7.0237)$	period $P \simeq 31.1$	1.1245	—
$7.0245 < d < 7.1980(7.2018)$	period $2P$	0.1745	8.2
$7.1980 < d < 7.2301(7.2341)$	period $4P$	0.321	5.4
$7.2301 < d < 7.2368$	period $8P$	0.0067	4.79

TABLE 3. The period-doubling cascade for the asymptotic problem $\Delta \to 0$, $R \to \infty$ with $\Delta R^{1/2} = d$. The period-doubling cascade found corresponds to a period-doubling of the relatively small second quasi-periodic frequency which enters as R_e increases for small Δ.

of the wall forcing so that the total flow is quasi-periodic. Thus for small Δ our calculations predict the onset of quasi-periodicity when

$$R = \frac{(5.99)^2}{\Delta^2} + \cdots, \tag{5.12}$$

and again this prediction is shown in figure 4. The numerical calculations for $\Delta = 0.25$ showed that quasi-periodicity began when $R \simeq 544$ whereas (5.12) gives $R \simeq 574$, in reasonably good agreement with the calculations.

If d is increased beyond $d = 5.99$ we observe a Feigenbaum period-doubling cascade to chaos. The results are shown in table 3. The corresponding figures given in Watson *et al.* are shown in brackets.

Note that Watson *et al.* say their results are unlikely to be correct to 3 significant figures so the agreement shown is as good as could be expected. We saw above that the streaming flow represented by ϕ becomes chaotic through the Feigenbaum route. At higher values of d our calculations always produced chaotic flows though it should be said that we did not carry out exhaustive searches for laminar subwindows. The value of the Feigenbaum constant predicted by our calculation is again close to the theoretical value. Poincaré cross-sections for runs at values of $d \geqslant 7.4$ show self-similar structures typical of chaotic flows. In the previous section we were reluctant to associate such structures with chaos but perhaps the results found in this section for the case $\Delta \ll 1, R \gg 1$ shed some light on that matter. By this we mean that the results for the case $\Delta = 0.25$ having a self-similar structure is a consequence of a period-doubling cascade on the second frequency which appears after the initial Hopf bifurcation. Thus we tentatively conclude that chaos occurs at all values of Δ at sufficiently large values of the Reynolds number. At moderate values of Δ this is a result of a period-doubling cascade associated with the period-of external forcing, and at lower values of Δ the cascade is associated instead with the modulational period. The difficulty in identifying conclusively a period-doubling cascade on the second frequency for finite but small Δ is that there, most of the energy is associated with the fast time scale, making it difficult to see a period-doubling cascade on the second frequency.

It is interesting to note that (5.8) and (5.9) with the sign changed on the boundary condition has a somewhat different structure when the forcing is increased. Note however that this situation does not apply to the internal steady streaming problem discussed here but is relevant to external steady streaming problems where the sign of the forcing is typically opposite to that found here; see Stuart (1966). In this case it turns out that there is once again a loss of symmetry at a finite forcing amplitude

followed by a Hopf bifurcation to a finite-amplitude periodic state. However a period-doubling cascade appears to be absent in this case though Watson *et al.* suggest that eventually the flow becomes chaotic. Calculations with our code suggested that in this case shock-like structures appear in the velocity time traces as the amplitude of the forcing increases.

Finally in this section we make some remarks about the finite-Δ, large-R limit. The calculations which we carried out and reported on in the last section all suggested that at sufficiently large values of the Reynolds number we should expect chaotic flows with laminar subwindows. When the Reynolds number is large, then, viscous boundary layers develop at the walls together with an inviscid core coupled to the motion in the nonlinear boundary layers. Unless the further limit of small Δ is taken little or no analytical progress can be made with the solution of the wall layer problems; therefore there is little simplification which can be made in the large-R, finite-Δ limit.

6. Conclusions

The present investigation began as an attempt to extend the instability analysis of Stuart *et al.* (1990) for squeeze bearing flows into the practically more relevant situation when the flow in the bearing is driven by the vibration of one of the walls. We found instead that time-periodic flows in squeeze bearings are unstable to perturbations having the same spatial structure as the basic state in the horizontal directions. Stuart *et al.* had investigated the possible instability to Tollmien–Schlichting waves of squeeze bearing flows but, on the basis of our knowledge of the instability of steady stagnation-point flows, see for example Hämmerlin (1956) and Dhanak & Stuart (1995), it might well be that vortex disturbances may be important also. We point out that the instabilities and chaotic flows which we have found may in practice be preceded by vortex or wave disturbances.

We found that for all values of the oscillation amplitude Δ the basic state which is known to be stable in the small Reynolds number limit loses stability at a finite value of R to a synchronous symmetry-breaking perturbation. The flow which develops beyond the first bifurcation point subsequently loses stability at a higher value of the Reynolds number to a disturbance which is no longer synchronous with the wall motion. At sufficiently large values of Δ the flow undergoes a period-doubling bifurcation following the well-known Feigenbaum scenario for the onset of chaos. At higher values of R the flow possesses laminar subwindows with rather unpredictable periods.

At sufficiently low values of Δ, after the second bifurcation the flow becomes quasi-periodic with the new frequency relatively small compared to the driving frequency. The motion beyond the second bifurcation sets in as a result of a Hopf bifurcation. Our calculations for the case $\Delta = 0.25$ suggest that chaos occurs at higher values of R. This was primarily suggested by the self-similar structures typical of chaotic flows which were found to exist in some of the Poincaré cross-sections. However, the presence of chaos was not immediately apparent in the frequency spectra which we calculated. The reason why this was the case was revealed by our asymptotic investigation of the small-Δ, large-R limit. Here we found that the flow essentially develops on two time scales, first the $O(1)$ time scale associated with the forcing and secondly a modulational time scale of size $O(R)$. On the longer time scale chaos occurs again as a result of a period-doubling cascade. We conjecture that this is also happening in the numerical simulations which we carried out for $\Delta = 0.25$ but the

detail of the breakdown is simply obscured by the much larger amplitude motion on the $O(1)$ time scale.

At the intermediate value of $\Delta = 0.45$ we found that the flow development had similarities with both the small- and large-Δ cases.The second bifurcation here was found to lead to a quasi-periodic flow in a similar manner to what was found for the $\Delta = 0.25$ case. However when the Reynolds number was increased further we found that the second frequency locked onto a value of $\frac{1}{4}$ of the driving frequency and a period-4π solution was established. However subsequent changes in R showed a development which was much harder to follow than was the case for the large-Δ simulations though we believe the cases to be essentially the same. For the $\Delta = 0.45$ case we found that after the period-4π solution was established the flow at higher values of R would stay chaotic for a successively increasing interval before reverting back to a period-4π solution. The chaotic attractor coexisting with period-4π solutions is more strongly attracting, and continuation methods were used to partially map out the subsequent development of the period-4π solution branches. Beyond certain Reynolds numbers, our continuation methods failed to converge to periodic solutions and converged to self-similar chaotic attractors instead. We believe that at higher values of R the flow will remain chaotic for all time and that again the chaos is associated with a period-doubling cascade. However, the nearness of the chaotic attractor to the period-4π solutions in phase space appears to make it impossible for us to map out this development.

Finally let us make some comments on the practical relevance of our analysis. We recall, see for example Secomb (1978), that the stagnation-point flow we have considered applies to the situation when a pressure gradient drives a flow in the x-direction. Thus our analysis gives an approximation for the size of wall vibrations which could cause loss of symmetry and ultimately chaotic flows in for example plane Poiseuille flow. In fact, if B denotes the physical wall amplitude of oscillation then our small-amplitude theory predicts loss of symmetry when

$$B = \frac{3.39\nu^{1/2}}{n^{1/2}} + \cdots .$$

Considering Poiseuille flow of water, for example, at a temperature of 20 °C (the kinematic viscosity being $\nu = 0.01\,\mathrm{cm^2\,s^{-1}}$), then wall vibrations of 1000 Hz, 100 Hz and 10 Hz respectively, require wall amplitudes of only about 0.06 mm, 0.2 mm and 0.6 mm to cause loss of symmetry and amplitudes of about 0.13 mm, 0.44 mm and 1.3 mm respectively to cause the onset of chaos. Using data from Secomb (1978), a fluid viscosity of $0.0346\,\mathrm{cm^2\,s^{-1}}$ and a frequency of vibration of 10 Hz, requires oscillation amplitudes of approximately 1.1 mm for loss of symmetry and 2.5 mm for onset of chaos. Typical vessel diameters used by Secomb are of the order of 12 mm or larger. (Note that we are applying the two-dimensional theory, but the axisymmetric geometries are expected to give analogous results.)

In the context of lubrication squeeze bearings, a similar estimate can be made for lubricating oils at bearing operating temperatures which can typically be of the order of 100 °C (see Hamrock 1991, for viscosity values of a range of lubricating oils). Using a 1000 Hz frequency of wall vibrations and a typical parafin base oil at 60 °C, 100 °C and 150 °C respectively, gives amplitudes of 0.23 mm, 0.14 mm and 0.09 mm respectively for loss of symmetry, and, 0.5 mm, 0.3 mm and 0.19 mm respectively for the onset of chaos. Similar results are found for other oils such as napthenic base oils or unused engine oils. We note that the estimated amplitudes are relatively small due to the decrease of viscosity with temperature.

The authors would like to thank the referees for constructive remarks on an earlier version of this paper. The work of D. T. P. was supported by the National Science Foundation (Grants DMS-970493 and DMS-9508298).

REFERENCES

Bergé, P., Pomeau, Y. & Vidal, C. 1984 *Order Within Chaos–Towards a Deterministic Approach to Turbulence*. Wiley-Interscience.

Brady, J. F. & Acrivos, A. A. 1981 Steady flow in a channel or tube with an accelerating surface velocity. An exact solution to the Navier–Stokes equations with reverse flow. *J. Fluid Mech.* **112**, 127–150.

Dhanak, M. R. & Stuart, J. T. 1995 Distortion of the stagnation-point flow due to cross-stream vorticity in the external flow. *Phil. Trans. R. Soc. Lond.* A **352**, 443–452.

Eckmann, J.-P. & Ruelle, D. 1985 Ergodic theory of chaos and strange attractors. *Rev. Mod. Phys.* **57**, 617–656.

Feigenbaum, M. 1979 The onset of spectrum turbulence. *Phys. Lett.* B **74**, 375–378.

Feigenbaum, M. 1980 The transition to aperiodic behavior in turbulent systems. *Commun. Math. Phys.* **77**, 65–86.

Gross, W. A. 1980 *Fluid Film Lubrication*. Wiley-Interscience.

Hall, P. 1978 The linear stability of flat Stokes layers. *Proc. R. Soc. Lond.* A **359**, 151–166.

Hämmerlin, G. 1956 Zur Theorie der dreimensionalen Instabilität laminarer Grenzschichten. *Z. Agnew. Math. Phys.* **7**, 156–164.

Hamrock, B. J. 1991 *Fundamentals of Fluid Film Lubrication*. NASA Reference Publication 1255, August 1991.

Papageorgiou, D. T. & Smyrlis, Y. S. 1996 Computer assisted study of strange attractors of the Kuramoto-Sivashinsky equation. *Z. Angew. Math. Mech.* **76**, 57–60.

Roux, J.-C., Simoyi, H. & Swinney, H. L. 1983 Observation of a strange attractor. *Physica* **8D**, 257–266.

Secomb, T. W. 1978 Flow in a channel with pulsating walls. *J. Fluid Mech.* **88**, 273–288.

Smyrlis, Y. S. & Papageorgiou, D. T. 1991 Predicting chaos for infinite dimensional dynamical systems: The Kuramoto–Sivashisnky equation, a case study. *Proc. Natl Acad. Sci. USA* **88**, 11129–11132.

Stuart, J. T. 1966 Double boundary layers in oscillatory viscous flows. *J. Fluid Mech.* **24**, 673–687.

Stuart, J. T., DiPrima, R. C., Eagles, P. M. & Davey, A. 1990 On the instability of the flow in a squeeze lubrication film. *Proc. R. Soc. Lond.* A **430**, 347–375.

Watson, E. B. B., Banks, W. H. H., Zaturska, M. B. & Drazin, P. G. 1990 On transition to chaos in two-dimensional channel flow symmetrically driven by accelerating walls. *J. Fluid Mech.* **212**, 451–485.